MOLECULAR PHYSICS, 1997, VOL. 92, NO. 3, 523–534

Electronic structures of the ground and excited states of $Mo(CO)_6$: SAC-CI calculation and frozen orbital analysis

By HIROSHI MORITA[1], HIROMI NAKAI[2], HIROYUKI HANADA[1] and HIROSHI NAKATSUJI[1,3,4]

[1] Department of Synthetic Chemistry and Biological Chemistry, Graduate School of Engineering, Kyoto University, Sakyo-ku, Kyoto 606-01, Japan
[2] Department of Chemistry, School of Science and Engineering, Waseda University, Shinjuku-ku, Tokyo 169, Japan
[3] Department of Applied Chemistry, Graduate School of Engineering, The University of Tokyo, Hongo, Tokyo 113, Japan
[4] Institute for Fundamental Chemistry, 34-4, Takano-Nishihiraki-cho, Sakyo-ku, Kyoto 606, Japan

(*Received 21 January 1997; accepted 26 April 1997*)

The symmetry adapted cluster (SAC) and symmetry adapted cluster–configuration interaction (SAC-CI) many body theories have been applied to calculate ground- and excited-state energies, and oscillator strengths of $Mo(CO)_6$. The experimental spectrum of $Mo(CO)_6$ is well reproduced by the present study, which is the first *ab initio* study of the excited states including electron correlations. The lower excited states are characterized as the metal-to-ligand charge-transfer (MLCT), ligand field transition (LFT) and Rydberg excitations. The LFT states are calculated to be much higher than the experimentally expected values. A new assignment based on the present calculations is proposed. The frozen orbital analysis (FZOA) method is applied to rationalize clearly the physical basis of the ordering of the excited states. This analysis is shown to be useful for understanding the excitation levels.

1. Introduction

The photochemistry of transition metal carbonyls has received much attention, largely because of their photocatalytic properties. The electronic structures of the ground and excited states of $Mo(CO)_6$ have also been studied experimentally and theoretically. The UV absorption spectra have been observed [1–3]. Beach and Gray have assigned their spectra using the extended Hückel calculation [3]. The lowest two peaks were assigned to the dipole-forbidden ligand field transition (LFT) states, namely, the d–d transition states. The upper two peaks (4·33 and 5·46 eV) were assigned to the dipole-allowed states. The assignment of the highest peak (6·39 eV) was never performed, probably because the calculations they used were only the extended Hückel level. Recently, Ho and co-workers have studied the photodissociation of $Mo(CO)_6$ on metal surfaces [4–8]: they compared the photodissociation yields of the adsorbed $Mo(CO)_6$ with the electronic spectra of the gaseous one [3].

On the theoretical side, the optimized geometry, the bond energy, and the vibrational frequency of $Mo(CO)_6$ were calculated by the density functional theory (DFT) [9–11]. These results are reliable for the ground electronic structure of $Mo(CO)_6$. However, there is no *ab initio* study for the excited states of $Mo(CO)_6$. Recently, Pierloot *et al.* [12] have studied the excited states of $Ni(CO)_4$ and $Cr(CO)_6$ using the CASPT2 method, which is a second-order perturbation method with a complete-active-space self-consistent field (CAS SCF) wave function, and reported that the LFT states were calculated to be much higher than the MLCT states. Beach and Gray assigned the lowest energy band of $Cr(CO)_6$ to the LFT state, as for $Mo(CO)_6$ [3]. Therefore, the assignment is different between the theoretical and experimental studies.

In this paper, we calculate the electronic structures of the singlet and triplet excited states of $Mo(CO)_6$, using the symmetry adapted cluster (SAC) [13]/SAC-CI [14] method. The accuracy and reliability of this method have been tested by numerous applications to diverse organic and inorganic systems [15], including the metal complexes like MO_4^{n-} (M = Ru, Os, Mn, Cr, Tc; $n = 0$, 1, 2) [16–19], TiX_4 (X = Cl, Br, I) [20, 21], CrO_2Cl_2 [22], $MoO_{4-n}S_n^{2-}$ ($n = 0$–4) [23], SnL_4 (L = H, CH_3) [24], $Ni(CO)_6$ [25], and MoF_6 [26, 27]. We want to give a

0026–8976/97 $12·00

reliable assignment of the observed peaks for $Mo(CO)_6$ and clarify the nature of the excited states. For $Ni(CO)_4$, we have studied the excitation spectrum and its photochemical decomposition reaction successfully using the SAC-CI method [25].

Since $Mo(CO)_6$ with O_h symmetry has degenerate MOs, many of the excited states, including both dipole-allowed and forbidden states, are due to the excitations between degenerate MOs. Although the forbidden excited states are difficult to observe directly by experiment, they are sometimes important in photochemical reactions. We have recently proposed the frozen orbital analysis (FZOA) method to clarify the ordering and splitting of the excited states having the same excitation nature [28]. In previous papers [27, 28], we have applied this method to the lower excited states of MoF_6 and $MoOF_4$. The lower excited states of MoF_6 and $MoOF_4$ are the ligand-to-metal charge-transfer (LMCT) excitations. In this paper, we show the analysis of the singlet and triplet excited states of $Mo(CO)_6$, characterized as the MLCT, LFT and Rydberg excitations. The FZOA method appears to be useful for understanding the chemical and physical nature of the excited states.

In section 2, we give technical details of the SCF and SAC/SAC-CI calculations. The geometry of $Mo(CO)_6$, basis sets, active MO space, and some principal features of the SAC-CI calculations are addressed shortly. Section 3 deals with the results for the ground and excited states and the orderings of the excited states of $Mo(CO)_6$. In section 4, we give concluding remarks and summarize the present work.

2. Computational details

The geometry of $Mo(CO)_6$ is that of the regular octahedron configuration. The experimental data was used for Mo–C and C–O bond parameters of 2·08 and 1·15 Å respectively [29]. The Gaussian basis set for the Mo atom is a (16s10p7d)/[7s3p4d] set of Huzinaga *et al.* [30] augmented with two p ($\zeta_p = 0{\cdot}081$, 0·026) functions [30] to represent the 5p orbital, Rydberg s ($\zeta_s = 0{\cdot}012\,01$, 0·005 856) and p ($\zeta_p = 0{\cdot}011\,04$, 0·005 455) functions [31]. For carbon, we use a (9s5p)/[4s2p] set of Huzinaga–Dunning [32] augmented with Rydberg s ($\zeta_s = 0{\cdot}023$) and p ($\zeta_p = 0{\cdot}021$) functions [33]. For oxygen, we use a (9s5p)/[4s2p] set of Huzinaga–Dunning [32]. The all-electron Hartree–Fock (HF) wave function for the ground state is calculated by using the program Hondo8 [34].

Electron correlations in the ground and excited states are taken into account by the SAC/SAC-CI theory [13, 14]. The active space in the SAC-CI calculations involves 21 higher occupied orbitals and 120 lower unoccupied orbitals calculated by the HF method. The 21 occupied orbitals are mainly composed of the 4d atomic orbitals of Mo and the 2p atomic orbitals of C and O. The 42 lower occupied and 15 higher unoccupied molecular orbitals (MOs) are neglected in the SAC-CI calculations.

In the SAC-CI calculations, all single-excitation operators are included in the linked term and double excitation operators are selected by the second-order perturbation method [35]. For the ground state, the double-excitation operators whose perturbation energy is larger than 3×10^{-5} hartree are included. For the excited states, the threshold of 4×10^{-5} hartree is used with respect to the main configurations ($C \geqslant 0{\cdot}1$) of 14 lower single excitation CI solutions for each symmetry.

In the SAC theory [35], the effect of the simultaneous binary collisions (four-body collisions) of electrons is dealt with in the form of the unlinked term. We include in the unlinked term all the double-excitation operators whose coefficients in the single and double (SD) CI are larger than 1×10^{-2}. In the SAC-CI theory [35], the transferable part of the electron correlation between the ground and excited states is expressed by the unlinked term. This term is expressed as the sum of double excitations from the main reference configurations of the state. These double excitations are those of which the SD-CI coefficients in the ground state are larger than 1×10^{-3}, and the main reference configurations are selected as those whose coefficients in the SD-CI are larger than 5×10^{-2}.

The SAC-CI calculations are performed with the use of the program SAC85 [36]. In the Appendix, we have investigated the dependence of the SAC-CI results on the basis set used, the active space, and the configuration selection.

3. Results and discussions

3.1. *SAC-CI calculations of $Mo(CO)_6$: ground and excited states*

The SCF MO energy sequence and their characters are shown in table 1, which involves only valence occupied and lower unoccupied orbitals up to the $15a_{1g}$ MO. In table 1, Mo(4d) and C(2p) denote the molybdenum 4d and C 2p atomic orbitals (AOs), respectively and Mo ± CO means bonding (+) and antibonding (−) combinations. The valence occupied orbitals from $9a_{1g}$ to $9t_{1u}$ MOs have the main characters of the ligand. The $3t_{2g}$ MOs are mainly due to molybdenum 4d AOs partially contributed by the $2p\pi^*$ orbitals of CO. In this respect, $Mo(CO)_6$ may be termed a d^6 complex.

As usual in metal–carbonyl compounds, the Mo–CO bond is explained by the σ donation and the π back donation. The electrons in the $2p\sigma$ of CO are denoted to 5s or 4d orbitals of Mo. Those in the 4d orbitals of Mo are back donated to the $2p\pi^*$ orbitals of CO. The

Table 1. Oribtal energies and characters of the HF wave function for $Mo(CO)_6$.

Symmetry	Character[a]	Orbital energy (au)
Occupied orbitals		
$9a_{1g}$	CO (2pσ) + Mo (5*s*); σ	−0·708 85
$2t_{2g}$	CO (2pπ); π	−0·674 03
$8t_{1t}$	CO (2pπ); π	−0·665 98
$5e_g$	CO (2pσ) + Mo (4d); σ	−0·663 44
$1t_{2u}$	CO (2pπ); π	−0·656 27
$1t_{1g}$	CO (2pπ); π	−0·650 55
$9t_{1u}$	CO (2pσ) + Mo (5p); σ	−0·603 97
$3t_{2g}$	Mo(4d) + Co(2pπ*); π	−0·344 70
Unoccupied orbitals		
$10a_{1g}$	Mo (6s) + C (3s); σ	0·008 24
$10t_{1u}$	Mo (6p) − C (3p); σ	0·010 54
$11t_{1t}$	Mo (6p) + C (3s); σ	0·034 72
$11a_{1g}$	Mo (6s) − C (3s); σ	0·035 56
$12t_{1u}$	CO (2pπ*) − Mo (5p); π	0·049 11
$6e_g$	C (3p) + Mo (4d); σ	0·055 23
$4t_{2g}$	C (3p) + Mo (4d); π	0·064 35
$13t_{1u}$	C (3s) − Mo (5p); σ	0·072 97
$2t_{2u}$	C (3p); π	0·084 01
$14t_{1u}$	C (3p) − Mo (5p); π	0·092 93
$3t_{2u}$	CO (2pπ*); π	0·094 29
$12a_{1g}$	Mo (5s) + C (3s); σ	0·097 25
$2t_{1g}$	C (3p); π	0·107 14
$13a_{1g}$	Mo (5s) + C (3p); σ	0·114 32
$7e_g$	C (3p) + Mo (4d); σ	0·137 24
$5t_{2g}$	CO (2pπ*) − Mo (4d); π	0·154 17
$3t_{1g}$	C (3p); π	0·165 80
$15t_{1u}$	C (3p) + Mo (5p); π	0·168 78
$16t_{1u}$	C (3s) − Mo (5p); σ	0·213 86
$14a_{1g}$	Mo (5s) − C (3s); σ	0·229 74
$8e_g$	Mo (4d) − CO (2pσ); σ	0·250 63
$17t_{1u}$	C (3s) − Mo (5p); σ	0·453 97
$6t_{2g}$	C (3p) − Mo (4d); π	0·473 13
93_g	C (3s) − Mo (4d); σ	0·491 44
$5a_{1g}$	C (3p) − Mo (5s); σ	0·498 43

[a] + and − denote bonding and antiboding combinations, respectively.

bonding orbitals of these interactions correspond to $9a_{1g}$ and $5e_g$ MOs for the σ donation and $3t_{2g}$ MOs for π back donation. The antibonding orbitals correspond to $8e_g$ MOs for the σ donation and $5t_{2g}$ MOs for the σ back donation. In this molecule, the virtual orbitals are composed of the CO 2pπ* orbitals, 4d AOs of Mo, and Rydberg orbitals. The $8e_g$ MO has largest amplitude in 4d AOs of Mo. The $12t_{1u}$, $3t_{2u}$, and $5t_{2g}$ orbitals have largest amplitude in the CO 2pπ* orbitals. The other unoccupied MOs in table 1 are Rydberg orbitals of C and Mo.

Table 2 shows the total energies, the Mulliken atomic orbital population, and the net charges of $Mo(CO)_6$ calculated by the HF and SAC methods. The correltion energy of −0·464 hartree by the SAC calculation is very large in comparison with the other systems [16–28]. The net charge of Mo atom is +1·228 and +1·320 at the HF and SAC methods respectively. The increase of the positive charge by including electron correlation is opposite to the cases for the d^0 complexes studied previously [16–23, 26–28]. Excitation configurations important for the ground-state electron correlation were the LMCT types in the d^0 complexes, while they are the MLCT type in the d^6 complex, $Mo(CO)_6$. This is the reason for the difference in the change of the metal charges. Since the π back donation for Mo to CO increases by electron correlation, the increase in the Mo charge means an increase of the covalency of the Mo–CO bond rather than that of the ionicity.

Table 3 gives a summary of the present SAC-CI results for the singlet excitation energy, main configuration, oscillator strength, second moment, and net charge for the calculated excited states below 7·2 eV. All main configurations of the excited states are single excitations from the $3t_{2g}$ MOs, in which the amplitudes are larger at 4d AOs of Mo than at ligand orbitals. These excited states are classified into three categories: namely, the MLCT, LFT and Rydberg excitations. The Rydberg excited states can be distinguished by using the second moment, which is the expectation values of r^2 and reflects the size of the electron-cloud distribution. The second moments for the ground and valence excited

Table 2. Total energy and the valence electron populations for the ground state of $Mo(CO)_6$ calculated by the HF and SAC methods.

Method	Energy/ hartree	Mo				C			O		
		s	p	d	charge	s	p	charge	s	p	charge
HF	−4648·541 076	+1·429	+0·371	−0·572	+1·228	+0·161	−0·125	+0·036	+0·166	−0·407	−0·241
SAC	−4649·005 087	+1·446	+0·358	−0·484	+1·320	+0·157	−0·194	−0·036	+0·167	−0·353	−0·185
Δ^a	−0·464 011	+0·017	+0·013	+0·088	+0·092	−0·004	−0·069	−0·072	+0·001	+0·054	+0·056

[a] The difference between HF and SAC values.

Table 3. Summary for the ground and singlet excited states of $Mo(CO)_6$.

State	Main configuration		Excitation energy/eV	Oscillator strength	Second moment	Net charge		
						Mo	C	O
X^1A_{1g}			0·0		2564	+1·31	−0·03	−0·18
1^1Eu	$3t_{2g} \rightarrow 12t_{1u}$	(MLCT)	4·509	0·0	2571	+1·83	−0·10	−0·20
1^1T_{2u}	$3t_{2g} \rightarrow 12t_{1u}$	(MLCT)	4·566	0·0	2571	+1·70	−0·08	−0·20
1^1A_{2u}	$3t_{2g} \rightarrow 12t_{1u}$	(MLCT)	4·593	0·0	2571	+1·79	−0·09	−0·19
1^1T_{1u}	$3t_{2g} \rightarrow 12t_{1u}$	(MLCT)	5·287	0·2927	2573	+1·59	−0·06	−0·19
2^1E_u	$3t_{2g} \rightarrow 3t_{2u}$	(MLCT)	5·594	0·0	2573	+1·77	−0·09	−0·20
1^1A_{1u}	$3t_{2g} \rightarrow 3t_{2u}$	(MLCT)	5·655	0·0	2573	+1·77	−0·09	−0·19
2^1T_{2u}	$3t_{2g} \rightarrow 3t_{2u}$	(MLCT)	5·887	0·0	2573	+1·72	−0·08	−0·20
1^1T_{2g}	$3t_{2g} \rightarrow 11a_{1g}$	(Rydberg)	6·047	0·0	2633	−0·73	+0·27	−0·15
1^1T_{1g}	$3t_{2g} \rightarrow 8e_g$	(LFT)	6·186	0·0	2570	+1·52	−0·07	−0·18
2^1T_{1g}	$3t_{2g} \rightarrow 5t_{2g}$	(MLCT)	6·432	0·0	2573	+1·60	−0·08	−0·18
1^1E_g	$3t_{2g} \rightarrow 5t_{2u}$	(MLCT)	6·440	0·0	2574	+1·58	−0·08	−0·18
2^1T_{2g}	$3t_{2g} \rightarrow 5t_{2g}$	(MLCT)	6·520	0·0	2574	+1·61	−0·08	−0·18
2^1T_{1u}	$3t_{2g} \rightarrow 11t_{1u}$	(Rydberg)	6·547	0·0801	2660	+0·28	−0·10	−0·15
3^1T_{2u}	$3t_{2g} \rightarrow 11t_{1u}$	(Rydberg)	6·594	0·0	2675	+0·22	+0·10	−0·14
2^1A_{2u}	$3t_{2g} \rightarrow 11t_{1u}$	(Rydberg)	6·621	0·0	2678	+0·31	+0·09	−0·14
3^1E_u	$3t_{2g} \rightarrow 11t_{1u}$	(Rydberg)	6·660	0·0	2682	+0·36	+0·08	−0·14
1^1A_{2g}	$3t_{2g} \rightarrow 3t_{1g}$	(MLCT)	6·772	0·0	2574	+1·73	−0·09	−0·19
3^1T_{1u}	$3t_{2g} \rightarrow 3t_{2u}$	(MLCT)	6·896	2·2320	2592	+1·61	−0·07	−0·19
3^1T_{2g}	$3t_{2g} \rightarrow 8e_g$	(LFT)	7·015	0·0	2594	+1·55	−0·08	−0·16
3^1A_{1g}	$3t_{2g} \rightarrow 5t_{2g}$	(MLCT)	7·215	0·0	2593	+1·66	−0·09	−0·18

states are from 2564 to 2594. The lowest one is for the ground state. On the other hand, the Rydberg states have larger values of second moments than the valence excited states, and these values are from 2633 to 2682. The 1^1T_{1g}, 2^1T_{1u}, 3^1T_{2u}, 2^1A_{2u}, and 3^1E_{2u} states can be assigned as the Rydberg states. The difference between the Rydberg and valence excitations can be also found in the net charges. The net charges of Mo for the valence excited states are from +1·55 to +1·83, whch are more positive than that for the ground state. On the other hand, those for the Rydberg states are from −0·73 to +0·36, more negative than that for the ground state.

Table 4 shows a summary of the triplet excited states calculated by the SAC-CI method. Similar to the singlet excited states, all the main configuration of the excited states lower than 6·5 eV are single excitations from the $3t_{2g}$ MOs. In the SAC-CI calculations, the triplet states have lower excitation energies than the signlet ones, known as Hund's rule. The ordering of the lowest four states having the $3t_{2g} \rightarrow 12t_{1u}$ excitation nature is different between the singlet and triplet states. The energy range of these states are smaller than that in the singlet state; namely, 4·23–4·51 and 4·51–5·29 eV, respectively. Similar tendencies are seen in the other excitation natures. The reason for this tendency is explained by the FZOA method [28] in the next section.

Table 5 shows the present assignment for the electronic spectrum of $Mo(CO)_6$ based on the SAC-CI calculations, in comparing with the previous experimental one by Beach and Gray [1, 3]. The electronic spectrum of $Mo(CO)_6$ is divided into four parts; namely, (I) first shoulder band, (II) second medium band, (III) third strong band, and (IV) fourth medium band.

The first weak shoulder band (I) was previously resolved into four components. The highest component of 4·05 eV was assigned to a spin-allowed LFT state, $^1T_{1g}$. The component of 3·81 eV was considered as the vibrational structure associated with the $^1A_{1g} \rightarrow {}^1T_{1g}$ transition. The assignment of the lowest component of 3·64 eV was a spin-forbidden LFT state, $^3T_{1g}$, because of its very weak intensity. The shoulder peak near 4·66 eV of the second band (II) was assigned to another spin-allowed LFT state, $^1T_{2g}$. However, the excitation energies of the corresponding $^3T_{1g}$, $^1T_{1g}$, and $^1T_{2g}$ states are calculated to be 5·87, 6·19, and 7·02 eV, respectively. Judging from the several tests in the Appendix, the errors of the present calculations are less than 0·3 eV. Therefore, the assignment for these weak peaks to the LFT states is suspect. It was also seen for the results of $Cr(CO)_6$ by Pierloot *et al.* [12] that the calculated LFT energies were much higher than the experimentally expected values. We assign the weak band (I) in the 3·6–4·0 eV region to the spin-forbidden 1^3T_{1u}, 1^3A_{2u},

Table 4. Summary for the triplet excited states of $Mo(CO)_6$.

State	Main configuration	Excitation energy/eV	Second moment	Net charge		
				Mo	C	O
X^1A_{1g}		0·0	2564	+1·31	−0·03	−0·18
1^3T_{1u}	$3t_{2g} \rightarrow 12t_{1u}$ (MLCT)	4·229	2571	+1·71	−0·09	−0·20
1^3T_{2u}	$3t_{2g} \rightarrow 12t_{1u}$ (MLCT)	4·336	2571	+1·73	−0·09	−0·20
1^3A_{2u}	$3t_{2g} \rightarrow 12t_{1u}$ (MLCT)	4·376	2571	+1·86	−0·11	−0·20
1^3E_u	$3t_{2g} \rightarrow 12t_{1u}$ (MLCT)	4·511	2572	+1·85	−0.11	−0·20
1^3A_{1g}	$3t_{2g} \rightarrow 5t_{2g}$ (MLCT)	5·316	2569	+1·63	−0·09	−0·19
2^2E_u	$3t_{2g} \rightarrow 3t_{2u}$ (MLCT)	5·582	2573	+1·76	−0·09	−0·20
2^3T_{1u}	$3t_{2g} \rightarrow 3t_{2u}$ (MLCT)	5·660	2573	+1·65	−0·08	−0·20
2^3A_{1u}	$3t_{2g} \rightarrow 3t_{2u}$ (MLCT)	5·689	2573	+1·75	−0·09	−0·20
2^3T_{2u}	$3t_{2g} \rightarrow 3t_{2u}$ (MLCT)	5·710	2573	+1·66	−0·08	−0·20
1^3T_{1g}	$3t_{2g} \rightarrow 8e_g$ (LFT)	5·865	2569	+1·52	−0·07	−0·19
1^3E_g	$3t_{2g} \rightarrow 5t_{2g}$ (MLCT)	5·872	2570	+1·61	−0·08	−0·18
1^3T_{2g}	$3t_{2g} \rightarrow 11a_{1g}$ (Rydberg)	5·989	2629	−0·60	+0·25	−0·15
2^3T_{2g}	$3t_{2g} \rightarrow 5t_{2g}$ (MLCT)	6·183	2572	+1·54	−0·07	−0·19
3^3T_{2g}	$3t_{2g} \rightarrow 8e_g$ (LFT)	6·379	2574	+1·46	−0·06	−0·18
3^3T_{1u}	$3t_{2g} \rightarrow 11t_{1u}$ (Rydberg)	6·540	2673	+0·26	+0·10	−0·14
2^3T_{1g}	$3t_{2g} \rightarrow 5t_{2g}$ (MLCT)	6·548	2576	+1·56	−0·07	−0·19

Table 5. Comparison between the previous experimental and present theoretical assignments of the electronic spectrum of $Mo(CO)_6$.

Experimental assignment[a]				Theoretical assignment			
ΔE/eV	Intensity	State	Main configuration	ΔE/eV	Intensity	State	Main configuration
(I) First shoulder band							
3·64	Very Weak	$^3T_{1g}$ (LFT)	$t_{2g} \rightarrow e_g$	4·23	spin-forbidden	1^3T_{1u} (MLCT)	$3t_{2g} \rightarrow 12t_{1u}$
3·81	Weak	Vibration		4·34	spin-forbidden	1^2T_{2u} (MLCT)	$3t_{2g} \rightarrow 12t_{1u}$
3·84	Weak	—		4·38	spin-forbidden	1^3A_{2u} (MLCT)	$3t_{2g} \rightarrow 12t_{1u}$
4·05	Weak	$^1T_{1g}$ (LFT)	$t_{2g} \rightarrow e_g$	4·51	spin-forbidden	1^3E_u (MLCT)	$3t_{2g} \rightarrow 12t_{1u}$
(II) Second medium band							
4·33	Peak	$^1T_{1u}$ (MLCT)	$t_{2g} \rightarrow t_{1u}$	4·51	dipole-forbidden	1^1E_u (MLCT)	$3t_{2g} \rightarrow 12t_{1u}$
~4·66	Shoulder	$^1T_{2g}$ (LFT)	$t_{2g} \rightarrow e_g$	4·57	dipole-forbidden	1^1T_{2u} (MLCT)	$3t_{2g} \rightarrow 12t_{1u}$
				4·59	dipole-forbidden	1^1A_{2u} (MLCT)	$3t_{2g} \rightarrow 12t_{1u}$
(III) Third strong band							
5·45	Peak	$^1T_{1u}$ (MLCT)	$t_{2g} \rightarrow t_{2g}$	5·29	0·2927	1^1T_{1u} (MLCT)	$3t_{2g} \rightarrow 12t_{1u}$
(IV) Fourth medium band							
~5·89	Shoulder	—		5·89	dipole-forbidden	2^1T_{2u} (MLCT)	$3t_{2g} \rightarrow 3t_{2u}$
6·39	Peak	—		6·55	0·0801	2^1T_{1u} (Rydberg)	$3t_{2g} \rightarrow 11t_{1u}$

[a] Reference [3].

and 1^3E_u, states, all being the MLCT arising from the $3t_{2g} \rightarrow 12t_{1u}$ transition.

The second medium band (II) at 4·33 eV was experimentally assigned to the dipole-allowed state, $^1T_{1u}$. The calculated excitation energy of 5·29 eV for the 1^1T_{1u} state is about 1 eV higher than the peak position. The position of the calculated 1^1T_{1u} state is closer to the third strong band (III) at 5·45 eV. The excitation nature of the 1^1T_{1u} state is the MLCT excitation and has a large intensity. In the energy range of the second band (II), there are three spin-allowed and dipole-forbidden states, 1^1E_u, 1^1T_{2u}, and 1^1A_{2u} states, which have the same excitation nature as the 1^1T_{1u} state. Therefore, we assign the third strong band (III) to the MLCT 1^1T_{1u} state and the second medium band (II) to the dipole-forbidden MLCT states.

The fourth medium band (IV) was not assigned by the previous experimental study. We assign it to the 2^1T_{1u} state calculated at 6·55 eV which is close to the peak position at 6·39 eV of this band. This state has a

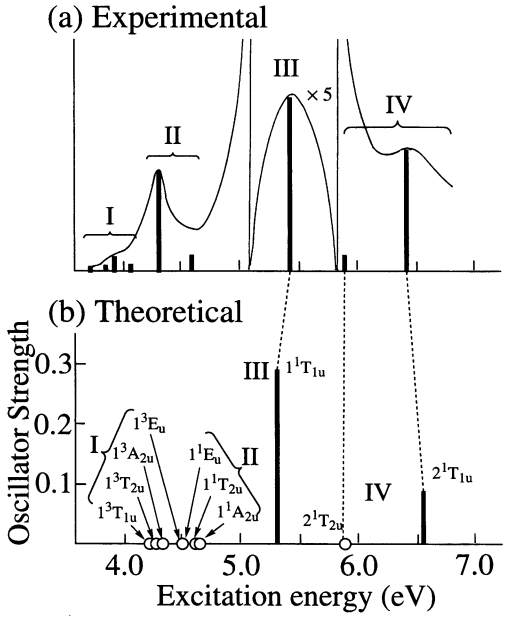

Figure 1. Experimental and theoretical electronic spectra of $Mo(CO)_6$. Experimenal spectrum is cited from [1].

Rydberg excitation nature. The calculated intensity of 0·08 is smaller than that of the MLCT 1^1T_{1u} state. The assignment of the 6·39 eV peak to the Rydberg 2^1T_{1u} state is new but quite natural.

The present calculations give eight dipole-forbidden states between the 1^1T_{1u} and 2^1T_{1u} states. There are various excitation natures of these states; namely, six MLCT, one LFT, and one Rydberg excitations. It is difficult to assign the shoulder peak of the fourth band (IV) to only one state, since they are all dipole-forbidden states. Based on the excitation energy, the 2^1T_{2u} state is close to the shoulder peak. However, this assignment is not confirmed. We propose that the resolution of the fourth band should be performed again with a more accurate electronic spectrum.

Figure 1 shows the comparison between the experimental and theoretical electronic spectra of $Mo(CO)_6$. The present theoretical spectrum shows a reasonable agreement with the experimental one.

3.2. *Frozen orbital analysis of $Mo(CO)_6$: excited states manifold*

In the preceding section, we showed the accurate SAC-CI results for the singlet and triplet excited states of $Mo(CO)_6$ and performed the assignment of the experimental electronic spectrum. Most of the calculated excited states are due to the excitations between degenerate MOs. For example, the 1^1E_u, 1^1T_{2u}, 1^1A_{2u}, and 1^1T_{1u} states have the same $3t_{2g} \rightarrow 12t_{1u}$ excitation nature. The energy split between the 1^1A_{2u} and 1^1T_{1u} state is not small; namely, 0·78 eV. The ordering of the four triplet states of the $3t_{2g} \rightarrow 12t_{1u}$ excitation is different from that of the singlet states. However, what determines the ordering and splitting of these excited states has never been clarified. For this purpose, we have recently proposed the frozen orbital analysis (FZOA) of the excited states [28].

First, we briefly explain the FZOA method. In O_h symmetry, there exist several triple degenerate MOs. One defines (ϕ_i, ϕ_j, and ϕ_k) and (ϕ_a, ϕ_b, and ϕ_c) as occupied and unoccupied degenerate MOs, respectively. The (ϕ_i, ϕ_a), (ϕ_j, ϕ_b), and (ϕ_k, ϕ_c) MOs are assigned to (b_{1u} or b_{1u}), (b_{2g} or b_{2u}), and (b_{3g} or b_{3u}) elements of D_{2h} symmetry, respectively. The excitations from (ϕ_i, ϕ_j, and ϕ_k) to (ϕ_a, ϕ_b, and ϕ_c) MOs lead to four distinct excited states, which are classified into the non-degenerate state A, the quadratic one E, and the two cubic ones T_+ and T_-. The + and − signs in the two cubic states correspond to those of the wave functions. In this paper, we write the singlet and triplet excitation energies in the following form;

$$\Delta E = A + B + C \qquad (1)$$

where A is the orbital energy difference, B is the $(-J + 2K)$ or $(-J)$ term, and C is the four-indices repulsion integral term. The B term brings about the energy splitting between (A, E) and (T_+, T_-) pairs. The C term further brings about the energy splitting between A and E and that between T_+ and T_-. Details are shown in [27, 28].

Figure 2 shows the energy levels for the singlet $3t_{2g} \rightarrow 12t_{1u}$, $3t_{2g} \rightarrow 3t_{2u}$, $3t_{2g} \rightarrow 5t_{2g}$, and $3t_{2g} \rightarrow 11t_{1u}$ excitations calculated by the FZOA and the SAC-CI methods. The ($12t_{1u}$, $3t_{2u}$, and $5t_{2g}$) and $11t_{1u}$ MOs have the valence and Rydberg unoccupied orbitals, respectively. The FZOA calculations cannot necessarily give quantitative results, since it actually corresponds to the single excitation (SE) CI calculation within the minimum active space [3 × 3]. However, the orderings of the four states by the FZOA method consistently agree with those of the SAC-CI method for the $3t_{2g} \rightarrow 3t_{2u}$ and $3t_{2g} \rightarrow 5t_{2g}$ excitations as shown in figure 2. In the excitations of $3t_{2g} \rightarrow 12t_{1u}$, the orderings in the pairs of (A, E) or (T_+, T_-) of the FZOA method are the same as the SAC-CI results. In the excitations of $3t_{2g} \rightarrow 11t_{1u}$, the splittings of the four states are very small and the orderings of these states are different between the FZOA and SAC-CI methods. We apply the FZOA method for understanding the complicated excited states of $Mo(CO)_6$ as used in MoF_6 [27, 28]. We also try to analyse why the $3t_{2g} \rightarrow 11t_{1u}$ excitation has very small splittings.

Table 6 lists the numerical data for the orbital energies and two-electron integrals appearing in the energy

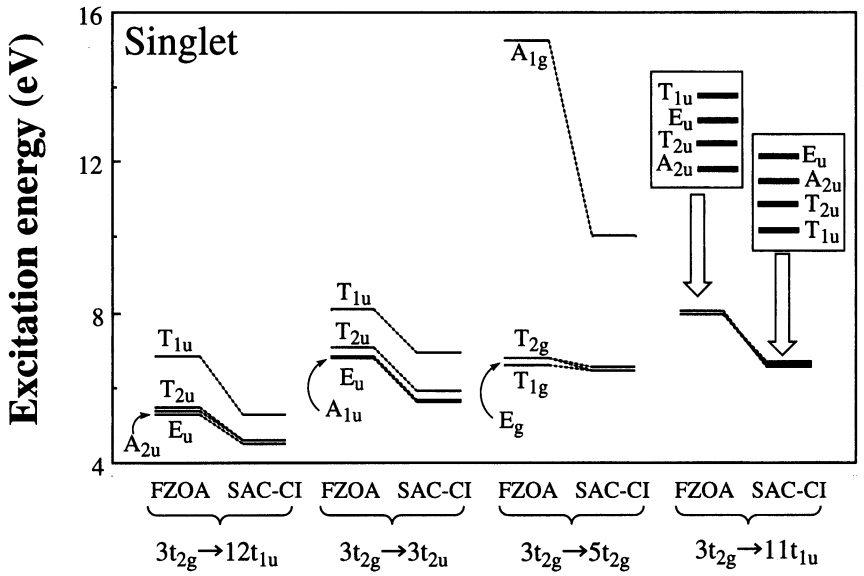

Figure 2. Comparison of the singlet excitation energies of the $Mo(CO)_6$ calculated by the FZOA and SAC-CI methods.

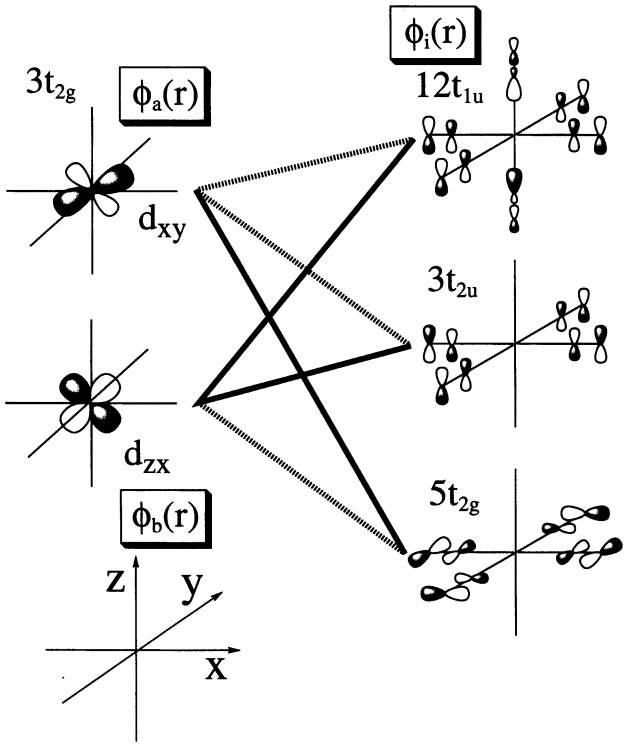

Figure 3. Combination of the orbitals for the transition density. The solid and dotted lines are large and small overlaps between them, respectively.

formula in [27, 28]. For $Mo(CO)_6$, the orbitals related to these excitations are all of the π-character. The difference between K_{ia} and K_{ib} and between $(ai|jb)$ and $(bi|ja)$ is the dominant factor in the ordering of these four states. From table 6, we see that the two exchange integrals K_{ia} and K_{ib} are different by an order of magnitude in every case. The integrals $(ai|jb)$ and $(bi|ja)$ are more important for the C term than the integrals $(ab|ij)$. They are also different by one order. The orderings of these integrals are equal; namely $K_{ia} > K_{ib}$, then $(ai|ja) > (bi|ja)$. These integrals include the transition density $\phi_a^*(r)\phi_i(r)$ or $\phi_b^*(r)\phi_i(r)$. The transition densities $\phi_j^*(r)\phi_b(r)$ and $\phi_j^*(r)\phi_a(r)$ involved in $(ai|jb)$ and $(bi|ja)$ have the same distributions as $\phi_a^*(r)\phi_i(r)$ and $\phi_b^*(r)\phi_i(r)$ respectively, besides the rotation of the coordinate axis. Therefore, the ordering of the integrals should be understood by analysing these transition densities. The transition density corresponds to the spatial distribution of the overlap between the two relevant MOs $\phi_a(r)$ and $\phi_i(r)$.

Figure 3 shows the schemtic illustration of the combinations $\phi_a^*(r) \times \phi_i(r)$ and $\phi_b^*(r) \times \phi_i(r)$ for the $3t_{2g} \rightarrow (12t_{1u}, 3t_{2u}, 5t_{2g})$ excitations. We here discuss the case of the $12t_{1u}$ MOs as an example. The $\phi_a(r)$ and $\phi_b(r)$ MOs with b_{1g} and b_{2g} symmetries have maximum amplitudes on the xy and xz planes respectively. On the other hand, the $\phi_i(r)$ MO with b_{1u} symmetry has a node on the xy-plane. Therefore, the pair of $\phi_i(r)$ and $\phi_b(r)$ has a larger overlap than that of $\phi_i(r)$ and $\phi_a(r)$. In figure 2, we show this overlap difference by using solid (large) and broken (small) lines, respectively. It turns out that the combinations $\phi_a^*(r) \times \phi_i(r)$ and $\phi_b^*(r) \times \phi_i(r)$ have larger overlaps for the gerade–gerade and ungerade–gerade pairs, respectively. This causes a large difference between $(ai|jb)$ and $(bi|ja)$, and further a large difference of the energy splittings between the E and A states and between the T_+ and T_- states. Since this also brings a large difference between K_{ia} and K_{ib}, the following general rule is proposed: *the larger-splitting states are higher in energy than the smaller-splitting.*

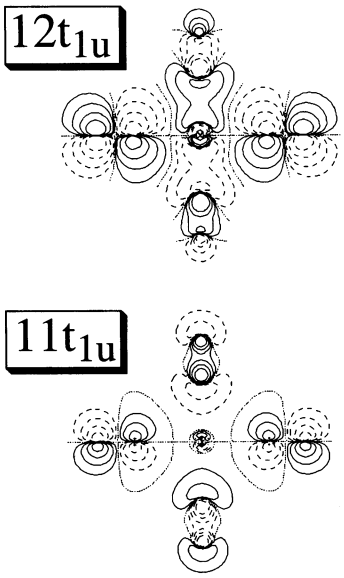

Figure 4. Contour maps of the $12t_{1u}$ and $11t_{1u}$MOs of $Mo(CO)_6$. Solid and broken lines correspond to plus and minus signs in the MO, respectively. The absolute values of the contours are 0·27, 0·09, 0·03 and 0·01.

Furthermore, since the transition density contributes to the intensity, we add a rule that the *dipole-allowed state has the larger splitting from other states and the highest energy*.

In figure 2, the splittings of the $3t_{2g} \rightarrow 11t_{1u}$ excitation is somewhat smaller than the other excitations. This is because the $11t_{1u}$ orbital is the Rydberg orbital. Figure 4 shows the MO maps of the $12t_{1u}$ and $11t_{1u}$ orbitals. The $11t_{1u}$ orbital has the sparse and widespread distribution of the electron cloud. The dense part of the electron cloud of the $11t_{1u}$ MO is more distributed in the area of each atom than that in $12t_{1u}$ MO. This indicates that the overlaps, both $\phi_a^*(r) \times \phi_i(r)$ and $\phi_b^*(r) \times \phi_i(r)$, are always small and all the integrals are rather small.

Next, the FZOA method is applied to the triplet excited states. Figure 5 shows the energy levels for the triplet $3t_{2g} \rightarrow 12t_{1u}$, $3t_{2g} \rightarrow 3t_{2u}$, and $3t_{2g} \rightarrow 5t_{2g}$ excitation states calculated by the FZOA and the SAC-CI methods. In the $3t_{2g} \rightarrow 5t_{2g}$ excitation, the orderings of the four states are kept in both methods. In the $3t_{2g} \rightarrow 12t_{1u}$ and $3t_{2g} \rightarrow 3t_{2u}$ excitations, the intrapair orderings between A and E or between T_+ and T_- are always kept in both methods. In figure 5, the splittings of the triplet excited states are smaller than those of the singlet excited states. In the triplet excited states, the dominant terms for the singlet state, K_{ia}, K_{ib}, $(ai|jb)$ and $(bi|ja)$ vanish from the energy formula. Only the J_{ia}, J_{ib} and $(ab|ij)$ integrals are included. As shown in table 6, the difference between J_{ia} and J_{ib} is small. The absolute values of $(ab|ij)$ are always small. This is the reason for the small splittings in the triplet states. The intrapair orderings between A and E or between T_+ and T_- are always opposite for the singlet and triplet states. This is explained by the $(ab|ij)$ integral having the same sign as the $(ai|jb)$ and $(bi|ja)$ integrals. Thus, the FZOA method is useful for understanding the singlet and triplet energy levels by the degenerate excitations.

4. Concluding remarks

We have applied the SAC/SAC-CI method to the calculations of the ground and excited states of $Mo(CO)_6$. We found that electron correlations in the ground state are very large partially because the back donation from Mo to C is large in this molecule. The electronic transitions below about 7·2 eV are character-

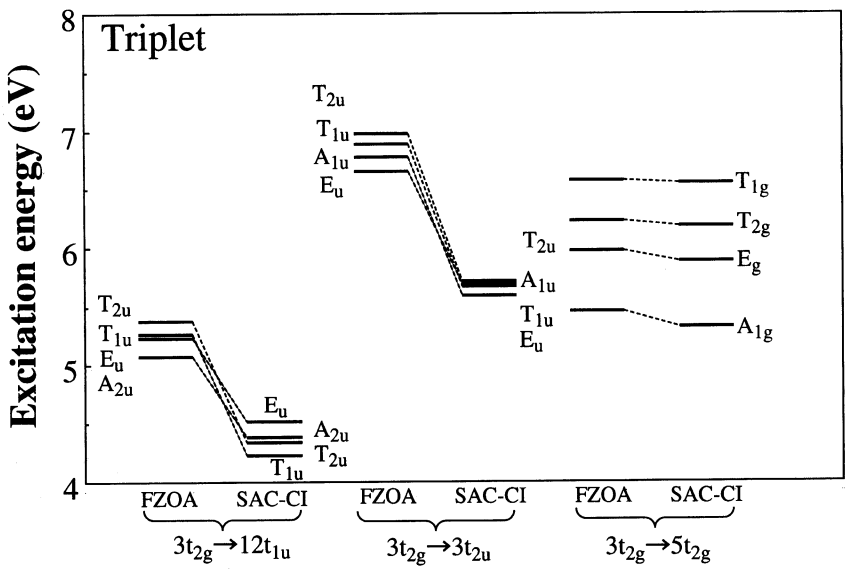

Figure 5. Comparison of the triplet excitation energies of the $Mo(CO)_6$ calculated by the FZOA and SAC-CI methods.

Table 6. Summary of the values of MO integrals of $Mo(CO)_6$ in the equation (1) (in eV).

Main configuration	State	*A* term			*B* term			*C* term			Transition dipole	
		ε_i	ε_a	Total	J_{ia} J_{ib}	K_{ia} K_{ib}	Total	$(ai\|jb)$ $(bi\|ja)$	$(ab\|ij)$	Total	$\langle\Phi_i^a\|r\|0\rangle$ $\langle\Phi_j^b\|r\|0\rangle$	Total
$3t_{2g} \rightarrow 12t_{1u}$ (MLCT)	$^1A_{2u}$	−9·3801	1·3363	10·7163	5·5415	0·0641	−5·4133	0·0461	0·0533	0·0780	0·0	0·0
	^1E_u	−9·3801	1·3363	10·7163	5·5415	0·0641	−5·4133	0·0461	0·0533	−0·0390	0·0	0·0
	$^1T_{1u}$	−9·3801	1·3363	10·7163	5·3974	0·4131	−4·5712	0·3709	0·0533	0·6884	1·3045	2·6091
	$^1T_{2u}$	−9·3801	1·3363	10·7163	5·3974	0·4131	−4·5712	0·3709	0·0533	−0·6884	1·3045	0·0
$3t_{2g} \rightarrow 3t_{2u}$ (MLCT)	$^1A_{1u}$	−9·3801	2·5659	11·9460	5·2131	0·0294	−5·1543	−0·0147	−0·0429	0·0268	0·0	0·0
	^1E_u	−9·3801	2·5659	11·9460	5·2131	0·0294	−5·1543	−0·0147	−0·0429	−0·0134	0·0	0·0
	$^1T_{1u}$	−9·3801	2·5659	11·9460	5·0177	0·3283	−4·3612	−0·2786	−0·0429	0·5143	1·1122	2·2244
	$^1T_{2u}$	−9·3801	2·5659	11·9460	5·0177	0·3283	−4·3612	−0·2786	−0·0429	−0·5143	1·1122	0·0
$3t_{2g} \rightarrow 5t_{2g}$ (MLCT)	$^1A_{1g}$	−9·3801	4·1953	13·5753	7·7820	1·8860	−4·0101	1·4951	0·1701	5·6404	0·0	0·0
	^1E_g	−9·3801	4·1953	13·5753	7·7820	1·8860	−4·0101	1·4951	0·1701	−2·8201	0·0	0·0
	$^1T_{1g}$	−9·3801	4·1953	13·5753	7·1766	0·1399	−6·8968	0·1392	0·1701	−0·1083	0·0	0·0
	$^1T_{2g}$	−9·3801	4·1953	13·5753	7·1766	0·1399	−6·8968	0·1392	0·1701	0·1083	0·0	0·0
$3t_{2g} \rightarrow 11t_{1u}$ (Rydberg)	$^1A_{2u}$	−9·3801	0·9448	10·3248	2·3978	0·0053	−2·3872	0·0038	0·0141	−0·0128	0·0	0·0
	^1E_u	−9·3801	0·9448	10·3248	2·3978	0·0053	−2·3972	0·0038	0·0141	0·0064	0·0	0·0
	$^1T_{1u}$	−9·3801	0·9448	10·3248	2·4257	0·0352	−2·3551	0·0310	0·0141	0·0479	0·3510	0·7019
	$^1T_{2u}$	−9·3801	0·9448	10·3248	2·4257	0·0352	−2·3551	0·0310	0·0141	0·0479	0·3510	0·0

ized as the MLCT, the LFT and the Rydberg excitations. The Rydberg states are distinguished by using the second moment and net charges of each atoms. The LFT states are calculated to be much higher than the experimental expected values. This is a very similar case to $Cr(CO)_6$ as studied by Pierloot *et al.* [12].

We give a new assignment of the electronic excitation spectrum of $Mo(CO)_6$ based on the present SAC-CI calculations. The lower two bands are assigned to the spin-forbidden and dipole-forbidden states, respectively. The excited states assigned to the lower two bands have all the $3t_{2g} \rightarrow 12t_{1u}$ configuration. The spin- and dipole-allowed state of the $3t_{2g} \rightarrow 12t_{1u}$ excitation nature is assigned to the third strong band. The fourth band, which has never been assigned previously, is found to correspond to the dipole-allowed Rydberg state. The present theoretical spectrum is in a reasonable agreement with the experimental one.

We have performed the analysis of the SAC-CI result using the FZOA method. The FZOA method is shown to be useful for analysing the ordering and the splitting of the valence excited states due to the excitations between the degenerate orbitals, although using the FZOA method it is rather difficult to determine the Rydberg excited states because of the small overlaps between the valence and the Rydberg orbitals. We have shown that the FZOA method is also useful for the triplet excited states.

Part of the calculations were performed at the Computer Center of the Institute for Molecular Science. This study has been partially supported by the Grant-in-Aid for Scientific Research from the Japanese Ministry of Education, Science, and Culture of Japan and by the New Energy and Industrial Technology Development Organization (NEDO) Agency of the Government of Japan.

Appendix: accuracy of the present calculation

We investigate the accuracy of the present SAC-CI calculations by using different basis sets, active orbital spaces, and thresholds for the configuration selection. Table A 1 shows the summary for several SAC-CI conditions and results. #0 corresponds to the condition adopted in the present study. We examine only singlet valence excitations. Rydberg bases of Mo and C are excluded in #1–#7. As shown later, it is found that the Rydberg bases are important even for calculating the valence excited states. The main differences among #1–#3 are the basis sets, with a change in the active unoccupied orbital space. The effects of a Mo f function and ligand polarization d functions are found in the results of #2 and #3, respectively.

The effect of the active occupied orbitals is examined by #1, #4, and #5. The active occupied orbitals of #1 consist of the 4d AOs of Mo and the 2p AOs of C and O, which are the same as #0. #4 further includes the 2s AOs of ligands, and #5 further involves the 4s and 4p AOs of Mo.

The thresholds for the configuration selection are $3{\cdot}0 \times 10^{-5}$ and $4{\cdot}0 \times 10^{-5}$ hartree for the ground and excited states, respectively, in both #0 and #1. More

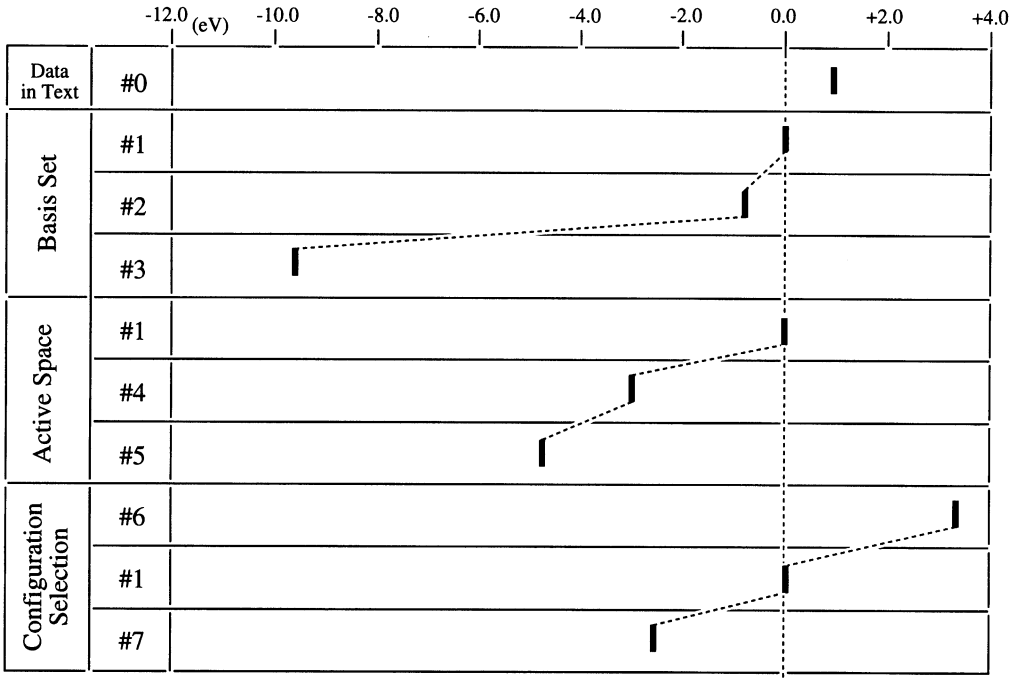

Figure A 1. Total energy of the ground state calculated by the SAC method with the conditions #0–#7. The energies are shown in eV relative to the result of #1.

crude and accurate thresholds are used in #6 and #7, respectively. The SAC-CI calculations are performed in the D_{2h} subset of the O_h symmetry. The numbers of the configurations after selection are shown in table A 1.

Figure A 1 shows the total energies of the ground state for the calculations #0–#7. The energy is shown relative to the #1 result. The addition of the Rydberg basis sets to MO and C give slightly higher energy. A reason is that the selected configurations in #0 are less than those in #1, using the same threshold. Comparing #1 and #2, we find that the addition of the f function to Mo does not bring a large change, but the result of #3 shows that the polarization d functions of the ligands are quite important for the total energy calculation. The results of #4 and #5 indicate that the electron correlations of the 2s AOs of ligands and the 4s and 4p AOs of Mo are not small. The effect of changing the threshold is also not small as found by comparing #6, #1, and #7.

Figure A 2 shows the singlet valence excitation energies obtained by the different SAC-CI calculations #0–#7. As mentioned before, the 1^1T_{2u}, 1^1E_u, and 1^1T_{1u} states have the MLCT nature, while the 1^1T_{1g} and 1^1T_{2g} states have the LFT nature. These excitation natures are never changed by the calculated conditions #0–#7.

The energy shifts by using #1–#7 are less than 0·1 eV for the 1^1T_{2u}, 1^1E_u, 1^1T_{1u}, and 1^1T_{2g} states. Even for the 1^1T_{1g} state, the shift is about 0·3 eV. These results may be surprising in comparison with the large shift in the ground-state energy shown in figure A 1. However, this small change in the excitation energy is reasonable and quite natural since most of the electron correlations in the ground state are transferable to the excited states. The SAC-CI method utilized this transferability of electron correlations effectively. Therefore, we estimate the error bars of the present excitation energies to be less than 0·3 eV.

Comparing between #0 and #1, we find that the Rydberg bases are important not only for the Rydberg excited states, but also for the valence excited states. Similar effects of the Rydberg bases were found for the valence states of ethylene [37] and benzene [38]. Namely, by adding the Rydberg bases, the valence and Rydberg spaces are divided and, as a result, the energy shifts of the valence states are brought about. This effect is larger in the LFT states than in the MLCT states. Furthermore, the energy shifts are opposite between the LFT and MLCT states. The three MLCT states shift by +0·15–+0·21 eV from #1 to #0. The energy shifts are about −0·17 and −0·45 eV for the LFT 1^1T_{1g} and 1^1T_{2g} states respectively. These results show that the Rydberg bases are important for the calculations of the valence states of $Mo(CO)_6$. However, it is expected that even if we add the Rydberg bases to #1–#7, the overall trends are not much modified.

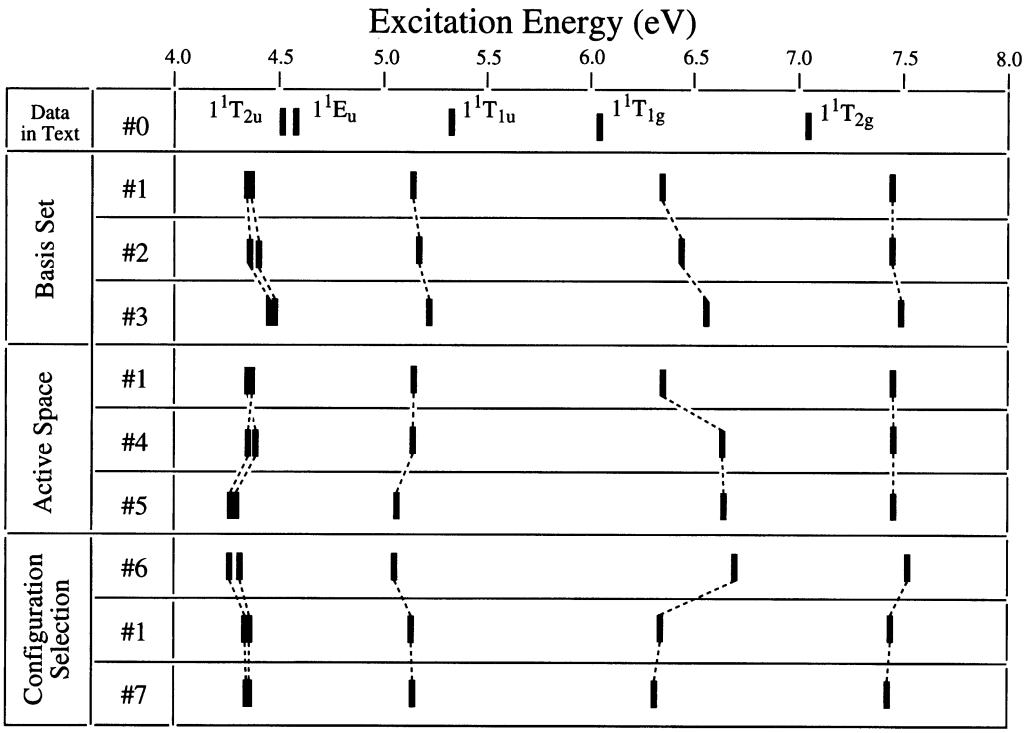

Figure A 2. Excitation energies calculated by the SAC-CI method with the conditions #0–#7. The energies are shown in eV.

Table A 1. Summary for the conditions and results in several SAC/SAC-CI.

Basic set	Active space	Threshold for selection	Number of configurations ^1A_g(g)	^1A_g(e)	^1A_u	$^1B_{1g}$	$^1B_{1u}$	Total energy/au[a] X^1A_{1g}	Excitation energy/eV[a] 1^1E_u	1^1T_{2u}	1^1T_{1u}	1^1T_{1g}	1^1T_{2g}
Data in text													
#0 Mo: [7s5p4d] + Ryd·[2s2p]	[21 × 120]	$\lambda_g = 3.0 \times 10^{-5}$	6764	21017	7091	18833	7676	−4649·012 62	4·509	4·566	5·287	6·186	7·015
C: [4s2p] + Ryd·[1s1p]	Mo 4d	(ground)						(+0·982)	(+0·162)	(+0·209)	(+0·150)	(−0·171)	(−0·449)
O: [4s2p]	C, O 2p	$\lambda_e = 4.0 \times 10^{-5}$											
Total: 194 AOs		(excited)											
Comparative calculations													
#1 Mo: [7s5p4d]	[21 × 86]	$\lambda_g = 3.0 \times 10^{-5}$	6911	18745	13956	16983	17835	−4649·048 72	4·347	4·357	5·137	6·357	7·464
C, O: [4s2p]	Mo 4d	$\lambda_e = 4.0 \times 10^{-5}$						(0·000)	(0·000)	(0·000)	(0·000)	(0·000)	(0·000)
Total: 162 AOs	C, O 2p												
#2 Mo: #1 + [1f]	[21 × 96]	Same as #1 (#0)	7307	20837	14374	17925	18759	−4649·077 37	4·388	4·400	5·173	6·419	7·461
C, O: Same as #1	Mo 4d							(−0·779)	(+0·041)	(+0·043)	(+0·036)	(+0·062)	(−0·003)
Total: 172 AOs	C, O 2p												
#3 Mo: Same as #1	[21 × 158]	Same as #1 (#0)	7481	22283	17221	20073	20992	−4649·402 52	4·454	4·446	5·210	6·549	7·487
C, O: #1 Pol·[1d]	Mo 4d							(−9·627)	(+0·107)	(+0·089)	(+0·073)	(+0·192)	(+0·023)
Total: 234 AOs	C, O 2p												
#4 Mo, C, O: Same as #1	[33 × 96]	Same as #1 (#0)	11280	26952	18313	23809	25932	−4649·162 23	4·356	4·349	5·127	6·625	7·465
Total: 162 AOs	Mo 4d							(−3·088)	(+0·009)	(−0·008)	(−0·010)	(+0·268)	(+0·001)
	C, O 2s,2p												
#5 Mo, C, O: Same as #1	[37 × 96]	Same as #1 (#0)	12292	28384	20681	25772	27568	−4649·223 35	4·283	4·283	5·074	6·655	7·459
Total: 162 AOs	Mo 4s,4p,4d							(−4·751)	(−0·064)	(−0·074)	(−0·063)	(+0·298)	(−0·005)
	C, O, 2s,2p												
#6 Mo, C, O: Same as #1	Same as #1	$\lambda_g = 1.0 \times 10^{-4}$	1928	9395	6839	8362	9040	−4648·914 71	4·287	4·270	5·045	6·690	7·508
Total: 162 AOs		$\lambda_e = 1.0 \times 10^{-4}$						(+3·646)	(−0·060)	(−0·087)	(−0·092)	(+0·333)	(+0·044)
#7 Mo, C, O: Same as #1	Same as #1	$\lambda_g = 1.0 \times 10^{-5}$	17270	29087	22541	27063	28319	−4649·138 70	4·323	4·323	5·140	6·313	7·425
Total: 162 AOs		$\lambda_e = 2.0 \times 10^{-5}$						(−2·448)	(−0·024)	(−0·034)	(+0·003)	(−0·044)	(−0·039)

[a] Energy differences from the #1 results are shown in parentheses (in eV).

References

[1] GRAY, H. B., and BEACH, N. A., 1963, *J. Amer. Chem. Soc.*, **85,** 2922.

[2] ALDERDICE, D. S., 1965, *J. Molec. Spectrosc.*, **15,** 509.

[3] BEACH, N. A., and GRAY, H. B., 1968, *J. Amer. chem. Soc.*, **90,** 5713.

[4] GLUCK, N. S., YING, Z., BARTOSCH, C. E., and HO, W., 1987, *J. chem. Phys.*, **86,** 4957.

[5] GERMER, T. A., and HO, W., 1988, *J. chem. Phys.*, **89,** 562.

[6] YING, Z. C., and HO, W., 1990, *Phys. Rev. Lett.*, **65,** 741.

[7] YING, Z. C., and HO, W., 1991, *J. chem. Phys.*, **94,** 5701.

[8] SO, S. K., and HO, W., 1991, *J. chem. Phys.*, **95,** 656.

[9] ZIEGLER, T., TSCHINKE, V., and URSENBACH, C., 1987, *J. Amer. Chem. Soc.*, **109,** 4825; Fan, L., and Ziegler, T., 1991, *J. chem. Phys.*, **95,** 7401; Li, J., SCHRECKENBACH, G., and ZIEGLER, T., 1994, *J. Phys. Chem.*, **98,** 4838.

[10] EHLERS, A. W., and FRENKING, G. J., 1994, *J. Amer. chem. Soc.*, **116,** 1514.

[11] DELLEY, B., WRINN, M., and LUTHI, H. P., 1994, *J. chem. Phys.*, **100,** 5785.

[12] PIERLOOT, K., TSOKOS, E., and VANQUICKENBORNE, L. G., 1996, *J. phys. Chem.*, **100,** 16 545.

[13] NAKATSUJI, H., and HIRAO, K., 1978, *J. chem. Phys.*, **68,** 2035.

[14] NAKATSUJI, H., 1978, *Chem. Phys. Lett.*, **59,** 362; Nakatsuji, H., 1979, *Chem. Phys. Lett.*, **67,** 329, 334.

[15] NAKATSUJI, H., 1997, *Computational Chemistry-Reviews of Current Trends*, Vol. 2, edited by J. Leszczynski (Singapore: World Scientific); NAKATSUJI, H., 1992, *Acta. Chim. Hung.*, **129,** 719.

[16] NAKATSUJI, H., and SAITO, S., 1991, *Int. J. quantum Chem.*, **39,** 93.

[17] NAKAI, H., OHMORI, Y., and NAKATSUJI, H., 1991, *J. chem. Phys.*, **95,** 8287.

[18] JIRSUHIRO, S., NAKAI, H., HADA, M., and NAKATSUJI, H., 1994, *J. chem. Phys.*, **101,** 1029.

[19] HASEGAWA, J., TOYOTA, K., HADA, M., NAKAI, H., and NAKATSUJI, H., 1995, *Theor. Chem. Acta*, **92,** 351.

[20] NAKATSUJI, H., EHARA, M., PALMER, M. H., and GUEST, M. F., 1992, *J. chem. Phys.*, **87,** 2561.

[21] NAKATSUJI, H., and EHARA, M., 1994, *J. chem. Phys.*, **101,** 7658.

[22] YASUDA, K., and NAKATSUJI, H., 1993, *J. chem. Phys.*, **99,** 1945.

[23] NAKATSUJI, H., and SAITO, S., 1990, *J. chem. Phys.*, **93,** 1865.

[24] YASUDA, K., KISHIMOTO, N., and NAKATSUJI, H., 1995, *J. phys. Chem.*, **99,** 12 501.

[25] HADA, H., IMAI, Y., HIDAKA, M., and NAKATSUJI, H., 1995, *J. chem. Phys.*, **103,** 6993.

[26] MORITA, H., NAKAI, H., TOMASELLO, P., and NAKATSUJI, H., 1996, *Bull. chem. Soc. Jpn.*, **69,** 1893.

[27] NAKAI, H., MORITA, H., TOMASELLO, P., and NAKATSUJI, H., unpublished.

[28] NAKAI, H., MORITA, H., and NAKATSUJI, H., 1996, *J. phys. Chem.*, **100,** 15753.

[29] WINTERS, R. E., and KISER, R. W., 1965, *Inorg. Chem.*, **4,** 157.

[30] HUZINAGA, S., ANDZELM, J., KLOBUKOWSKI, M., RADZIO-ANDZELM, E., SAKAI, Y., and TATEWAKI, H., 1984, *Gaussian Basis Sets for Molecular Calculations* (New York: Elsevier).

[31] JUNGEN, M., 1981, *J. chem. Phys.*, **74,** 750.

[32] DUNNING, JR, T. H., 1970, *J. chem. Phys.*, **53,** 2823.

[33] DUNNIG JR, T. H., and HAY, P. J., 1977, *Modern Theoretical Chemistry*, Vol. 3, edited by H. F. Schaeffer III (New York: Plenum).

[34] DUPUIS, M., and FARAZDEL, A., 1991, Program System HONDO8 from MOTECC-91.

[35] NAKATSUJI, H., 1983, *Chem. Phys.*, **75,** 425.

[36] NAKATSUJI, H., 1985, Program System for SAC and SAC-CI calculations, Program Library No. 146 (Y4/SAC), Data Processing Center of Kyoto University; 1986, Program Library SAC85, No. 1396, Computer Center of the Institute for Molecular Science.

[37] NAKATSUJI, H., and KITAO, O., 1988, *Chem. Phys. Lett.*, **143,** 528.

[38] KITAO, O., and NAKATSUJI, H., 1987, *J. chem. Phys.*, **87,** 1169.